



# Analysis of the First Cosmic Ray Data Collected with the Complete ALICE TPC

Philippe Gros

October 2006 - February 2007

Master Project in Physics
École Polytechnique Fédérale de Lausanne

Supervisors :
in Sweden : Peter Christiansen
in Switzerland : Aurelio Bay



**Abstract**

The Large Hadron Collider (LHC), which will soon be operational at CERN, will provide a powerful tool to study particle physics. With 14TeV proton-proton collision at a luminosity of $10^{34}\mathrm{s}^{-1}$ $\mathrm{cm}^{-2}$, it will be by far the most powerful accelerator ever built. It will allow experiments such as ATLAS, CMS and LHCb to test the limit of the Standard Model and to find evidence of new physics such as SUperSymmetrY (SUSY). It will also be possible to recreate one of the first phases of the early Universe, to study the hadronic matter under extreme conditions of temperature and density. This is the purpose of ALICE (A Large Ion Collider Experiment), which will study the Quark Gluon Plasma (QGP) created in collisions of heavy ions at LHC.

The study of this very interesting but very ephemeral medium requires a complex detection apparatus. One of the main detectors, the Time Projection Chamber (TPC) will track all the charged particles emitted in a region around mid-rapidity. The very high track density expected makes this an ambitious project.

The TPC construction has recently been completed and the TPC is currently down in the ALICE pit ready to be installed. The first tests of the complete TPC have been done with cosmic rays and laser tracks, and are now studied to understand and optimise the operating configuration and the data processing software.

In this thesis I present results of studies I carried out of the first cosmic data. I focused on selected runs to identify the flaws in the data.

Some of the results shown here were presented at the first ALICE Nordic collaboration meeting in Copenhagen and the ALICE TPC meeting at GSI, Darmstadt.

# Contents

# Chapter 1

# Relativistic Heavy Ion Physics

The ALICE experiment at LHC is optimised for the study of heavy ion collisions. Heavy ions such as gold (Au) and lead (Pb) are collided to study the properties of extremely hot and dense matter. This matter will mainly be composed of quarks and gluons, which behave according to Quantum ChromoDynamics (QCD). In the chapter some of the important properties of QCD and quark confinement will be reviewed and finally the notion of QGP will be described.

## 1.1 QCD

### 1.1.1 Quark Model

In the Standard Model, matter is described with a few fundamental particles : quarks, leptons and gauge bosons. These particles carry charges which define their interactions. The quarks have electric charge ($-\frac{1}{3}$ or $+\frac{2}{3}$) and flavor ($u$ (up), $d$ (down), $c$ (charm), $s$ (strange), $t$ (top), $b$ (bottom)). But contrarily to the leptons, they also carry a "colour" charge (red, green or blue), which gives rise to Strong Interaction described by QCD. In addition, all these particles have their symmetric anti-particle with opposed charges (for example an anti $u$-quark has charge $-\frac{2}{3}$ and anti-colour).

In the same way as electromagnetic interaction tends to bring together opposed electric charges so that environment be electrically neutral, the Strong interaction brings quarks together so that the environment is colourless. However, unlike in electromagnetism (QED), there are two kinds of neutralities :

**Baryon** three quarks of the three colours (e.g. proton)

**meson** a quarks and an anti-quark of colour and anti-colour (e.g. pion).

Another important difference with electromagnetism is that the interaction boson, the gluon, also carries colour charge, unlike the photon which is electrically neutral. The coloured gluon gives rise to the exotic properties of QCD described in the next sections.

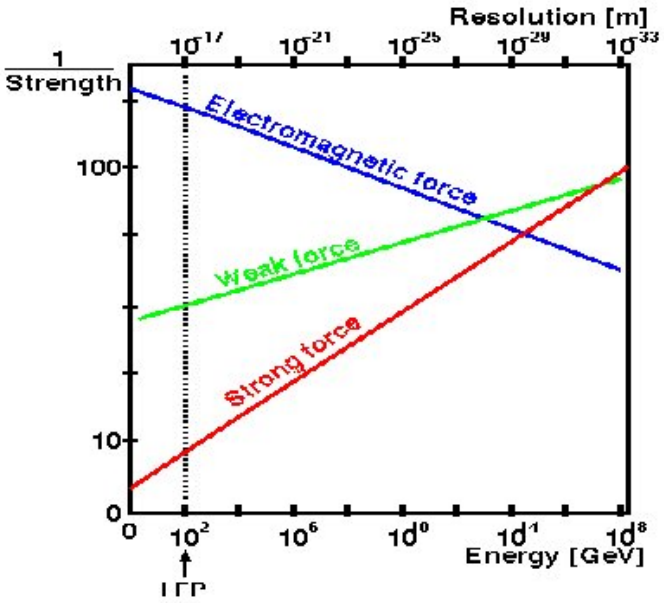


Figure 1.1: Running of the coupling constants with energy transfer

### 1.1.2 Confinement

The Strong interaction is so strong that quarks have never been observed individually. The quarks remain confined inside hadrons. The Strong potential, contrarily to the Coulomb potential does not fade at large distances. Much like with an elastic, the more the quarks are brought apart, the stronger is the force that links them. A simple approximation of the Strong potential (in the case of heavy quarks) is :

$$V(r) = \sigma r + \frac{\epsilon}{r} \tag{1.1}$$

which means that at short distances, it resembles a Coulomb potential, and at large distances the potential grows linearly with the separation distance. The "string" constant $\sigma$ is of the order of 1 GeV/fm.

If two quarks of opposed colour are pulled apart, the "string" between them will eventually "break" when the amount of energy contained in the string is large enough for the creation of new quarks that will maintain the colour neutrality.

### 1.1.3 Asymptotic Freedom

Another way of characterising an interaction is through the coupling constant. The coupling constant describes the strength of an interaction, and allows to calculate cross-sections in *perturbative QCD* (pQCD). For the perturbative expansion to converge, the coupling parameter must be small, which is the case for QED, where the coupling constant is called the fine structure constant $\alpha \approx \frac{1}{137}$. In fact, the coupling constants depend on the energy of the interaction and the electromagnetic coupling constant grows with energy (Figure 1.1). The strong coupling constant decreases with energy transfers. At low energy transfer (below

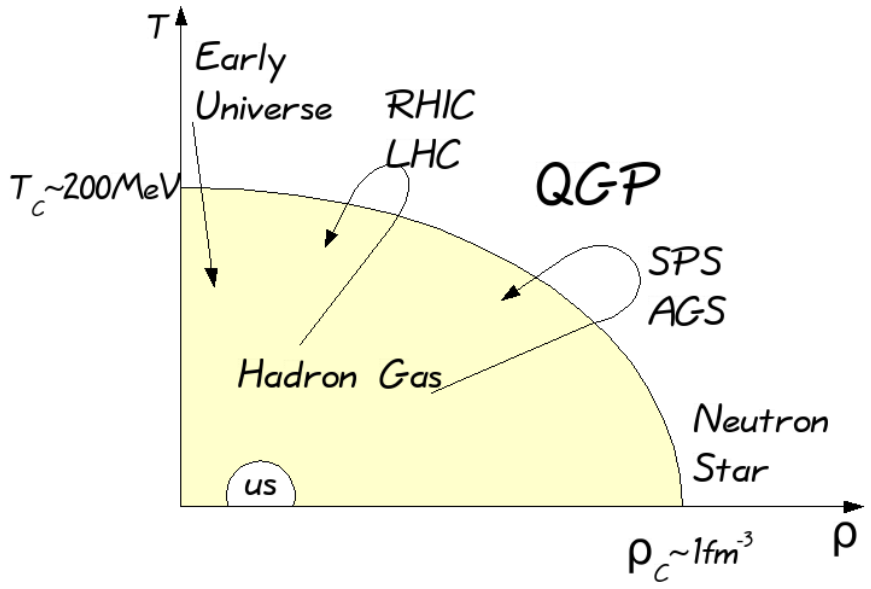


Figure 1.2: Trajectories in the $(\rho, T)$ plane of early Universe, Neutron stars and experimental ion collisions

200MeV), it is greater than one, which reflects that at large distances, the interaction is very strong and leads to quark confinement. As perturbative approach is not possible, one has to rely on numerical calculation on a lattice (LQCD). For high energies (short distances), the coupling constant becomes small enough to use pQCD. Inside hadrons, the quarks appear to be free : this is often called *asymptotic freedom*.

## 1.2 Quark-Gluon Plasma

In LQCD calculations [6], it is observed that at temperature around 170MeV there is a phase transition where the number of degrees of freedom ($DoF$) grows enormously. The new phase of matter is called Quark Gluon Plasma (QGP). The hadronic degrees of freedom are dominated by the 3 pions ($\approx 3DoF$), while in a QGP the degrees of freedom are light quarks, anti-quarks and gluons ($\approx 40DoF$).

If we compress normal matter (i.e. protons and neutrons), the quarks inside the hadrons will not be able to keep their identity and instead form a soup of quarks. This transition should happen when the distance between the hadrons is smaller than their size ($\approx 0.8$fm). In a QGP, the collective behaviour of the quarks should be different from hadronic system, and give information about the Strong interaction.

A simple phase diagram of hadronic matter can thus be drawn, which looks like figure 1.2.

In heavy ion collisions we make excursions in this diagram. Astrophysical and cosmological phenomena, such as the core of dense neutron stars are other

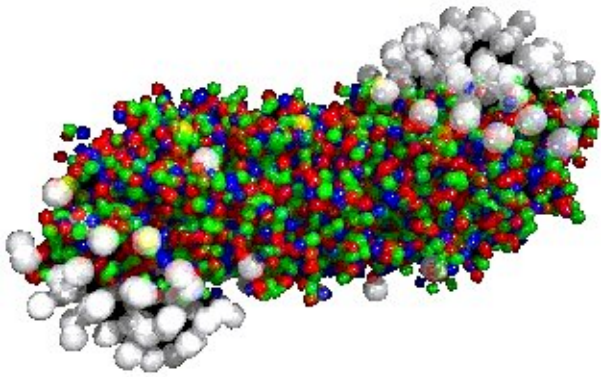

areas where QGP might exist.

### 1.2.1 History of the Universe

Study of the QGP will give a better understanding of the history of the Universe. In the Big Bang theory, the Universe was created as an extremely hot and dense soup of matter. It then expanded and cooled down to become the Universe as we know it today. As it cooled down matter went through different states, or different phases to speak with thermodynamical terms. The QGP is one of the earliest of these phases (the first microseconds), and understanding it can give more indications about how this phase affected the evolution of the Universe. It will of course also give a better understanding of the strong interaction, and thus a better understanding of the way nature works...

### 1.2.2 Heavy Ions Collisions : a Tool to Study the QGP

As we have seen, the QGP is a "macroscopic" (compared to a single baryon) state of quarks and gluons in thermodynamical equilibrium with extremely high temperature. The conditions to create such a state are probably reached at the centre of some stars (neutron stars) but this is very difficult to observe. On Earth, to obtain a "macroscopic" medium, with a lot of constituents, heavy ion (lead or gold) collisions are used. To bring the system to a high enough temperature, the nuclei are collided at very high energy (hundreds of GeV per nucleon pair).

To reach the conditions to create a QGP, the two colliding nuclei's must have a large overlapping cross-section area. The impact parameter is therefore an important parameter in the analysis of heavy ion collisions, since only a small fraction of the events will correspond to central collision. The collision with a small impact parameter will hopefully create QGPs, while the very peripheral may still give interesting $p + p$-like data of hot hadronic matter to which the QGP behaviour can be compared.

### 1.2.3 Experimental signatures of a QGP

The production of a QGP should be possible if the energy density reached in the collisions is large enough. But once we have a QGP, the challenge is first

to identify it, and then to probe it and study its properties. There are several aspects that can be seen as evidence of the creation of a QGP. Here are the main expected probes of a QGP.

**Elliptic flow** In non-central collisions, the overlap section is elliptical and the density gradient is non-uniform. In the case of a QGP with very strong early interaction, this should influence the distribution of the emitted particles, while in hadronic matter, particles should not have time to interact inside the medium. Some hydrodynamic models of an ideal partonic fluid have been able to describe data from RHIC [6].

**High $p_T$ particles** At large momentum transfer, pQCD is applicable and predicts the production of jets in $p + p$ collisions. The number of high $p_T$ hadrons produced in heavy ions collisions at RHIC is lower than expected, while photons behave as expected. This "jet quenching" is thought to be due to energy loss in the very dense medium. This energy loss is due to strong interaction, which is why it doesn't affect photons. Therefore, the study of high $p_T$ particles and jet quenching will give hints about the density and properties of the QGP.

**$J/\psi$ suppression** The $J/\psi$ is a bound state of quark and anti-quark, $c\bar{c}$. In a QGP, the dense colour environment should screen the potential between $c$ and $\bar{c}$, and the $J/\psi$ should then dissolve in the medium. The subsequent $J/\psi$ suppression is now one of the most intriguing signatures of the creation of a QGP at SPS.

## 1.3 From RHIC to LHC

The RHIC (Relativistic Heavy Ions Collider) at Brookhaven, USA, collides gold (Au) ions with a centre of mass energy per nucleon pair $\sqrt{s_{NN}}$ of up to 200 GeV, and has 4 specialised experiments (BRAHMS, PHENIX, PHOBOS and STAR). These experiments gave over the last few years a lot of exciting results about heavy ions physics and have found indications for the creation of a strong interacting QGP that behaves as a near perfect fluid.

The 5.5 TeV per nucleon Pb+Pb collisions in LHC represent a big leap in energy scale. As the temperature and density of the medium created in the collision will greatly increase, hopefully giving clearer evidence of QGP, the complexity of the data produced will make it more difficult to study. The ALICE experiment developed complex and very precise detectors to meet this challenge.

# Chapter 2

# The ALICE TPC

## 2.1 LHC

At CERN in Switzerland the Large Hadron Collider (LHC) is under construction. It will start operating at the end of 2007. The LHC will be by far the most powerful particle accelerator ever built. It will be able to accelerate protons up to a centre of mass energy of 14TeV, and heavy ions with an energy of 5.5TeV per nucleon pair. This is a great opportunity to search for new physics.

### 2.1.1 $p-p$ Physics

The experiments ATLAS, CMS and LHCb are expected to give exciting new results. They will use 14TeV proton-proton collisions with high luminosity to look for rare events. ATLAS and CMS aim at discovering and study the *Higgs boson*, involved in the mass creation mechanism. The Higgs is the most important particle in the Standard Model that has not yet been observed. The search for direct signatures of new particles such as those predicted by SUperSymmetrY (SUSY) is also a major program. LHCb will focus on $b$-quarks physics to establish with unpreceeded precision the parameters of the CKM matrix and to try to discover new physics beyond the Standard Model. This should appear for example in the form of new particles (e.g. SUSY particles) which, though not directly seen, will modify Feynman diagrams and therefore give reactions or cross sections different from the Standard Model predictions.

### 2.1.2 Heavy Ion Physics

ALICE (A Large Ion Collider Experiment) is optimised for the study of the QGP in heavy ions collisions at LHC. These collisions are expected to produce an enormous amount of particles (tens of thousands of them should be detected in the detection apparatus).

The purpose of the experiment is to study the QGP phase of matter. It is therefore designed to study in detail every collision which will create a QGP. Heavy ion collisions will have a very small rate compared to other LHC experiments (about a few thousands events per second, compared to millions for an experiment like ATLAS). However, almost every collision should bring interesting data, while the other experiments look for very rare events, so ALICE can

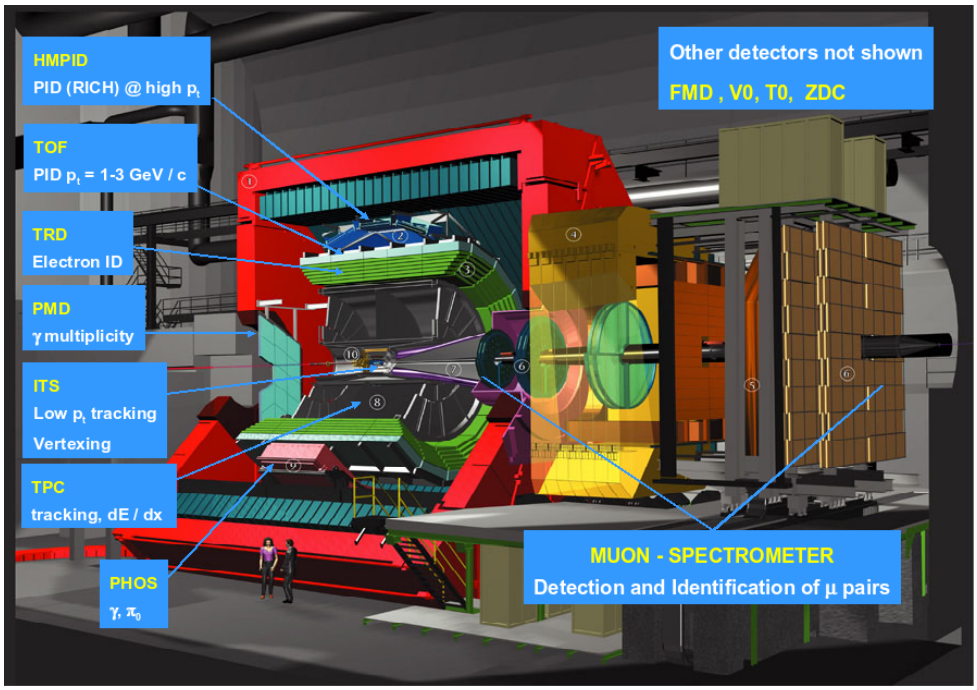


Figure 2.1: The ALICE Experiment

use slower detectors to measure precisely the outcome of a collision.

I will now briefly describe the detection apparatus of ALICE. I will then focus on the TPC, and the data it will provide.

## 2.2 Detector Configuration

In order to study a QGP, ALICE must gather a lot of information about what happens in the collision. For this purpose, it has a set of detectors which will identify the particles emitted and their trajectories, which should allow to determine what really happened in the collision. ALICE consists of a central barrel detector inside the L3 magnet and a muon arm with a dipole magnet. In addition to these two main detector systems there are forward detectors for the determination of the interaction point, the event plane and the centrality.

Here we will focus on the central barrel. It has a characteristic "onion" structure, in which can be found the following detectors.

**The Inner Tracking System (ITS)** consists of six cylindrical layers of silicon detectors, wrapped around the beam pipe at the nominal interaction point. It is part of the tracking system and pin-points the position of the collision to the precision of tens of micrometres. The ITS is important to identify the decay vertices of e.g. heavy quarks.

**The Time Projection Chamber (TPC)** will be described more precisely in the next section.

**The Transition Radiation Detector (TRD)** can discriminate electrons from other charged particles using the emission of transition radiation – x-rays emitted when the particles cross layers of thin materials. This is important to reconstruct leptonic decays of resonances.

**The Time of Flight (TOF)** identifies pions, kaons and protons by the time they take to cover the distance between the collision point and the detector. It consists of layers of multigap resistive plate chambers (MRPC).

**The High Momentum Particle Identification (HMPID)** is used to identify fast-moving particles (protons and kaons can be separated up to 5 GeV/c). In the $C_6F_{14}$-radiator, they emit Cherenkov light. The photons are detected by a thin CsI layer deposited on the pad plane of a MultiWire Proportional Chamber (section 2.3.2). The radius of the Cherenkov rings will allow to identify the particles.

**The Photon Spectrometer (PHOS)** is made of lead tungstate crystals, a material so dense that it can stop most photons that reach it. When the photons strike the lead tungstate, they create electronic showers that will then be detected and from the characteristics of which the momentum of the photon will be extracted. It is designed to detect direct and decay photons from the medium, and measure some very high momentum particles ($\pi^0$, $\delta$).

## 2.3 Main Tracking Device : the TPC

The TPC is the main tracking device in the central barrel. It will measure the trajectories of the charged particles, and it is designed to identify tracks of up to 20 000 particles (primary and secondary) in each collision. By identifying the momentum and energy loss, it will be able to identify particles with low momentum ($< 1$ GeV/c) and hopefully also with momentum in the range of 3-20 GeV/c ($e^{\pm}$, $\pi^{\pm}$, $K^{\pm}$ and $p^{\pm}$). It is a big and precise detector, but it is slow. Each measurement takes about 100 $\mu s$, but it is consistent with the interaction rate in Pb+Pb of 1kHz.

### 2.3.1 Operation Principle

The ALICE TPC is a hollow cylinder (see fig. 2.2), 5m diameter and 5m long, filled with Ne-$CO_2$ (90-10). Inside the TPC field cage a strong axial electric field is generated by a central high voltage (100kV) electrode. When a charged particle crosses the chamber, it will ionize the gas. The freed electrons will then drift along the electric field lines toward the readout chambers (MultiWire Proportional Chambers MWPC) located at both ends of the field cage. The constant drift velocity of the electrons will give a simple relation between their arrival time and the original axial position of the ionization. The charge, position and arrival time are recorded by the readout chambers and will allow the point from which the electrons originated to be reconstructed, and thus the trajectory of the ionizing particle to be measured. The number of electrons coming from one track segment will be proportional to the energy loss of the ionizing particle and can be used to identify the particle.

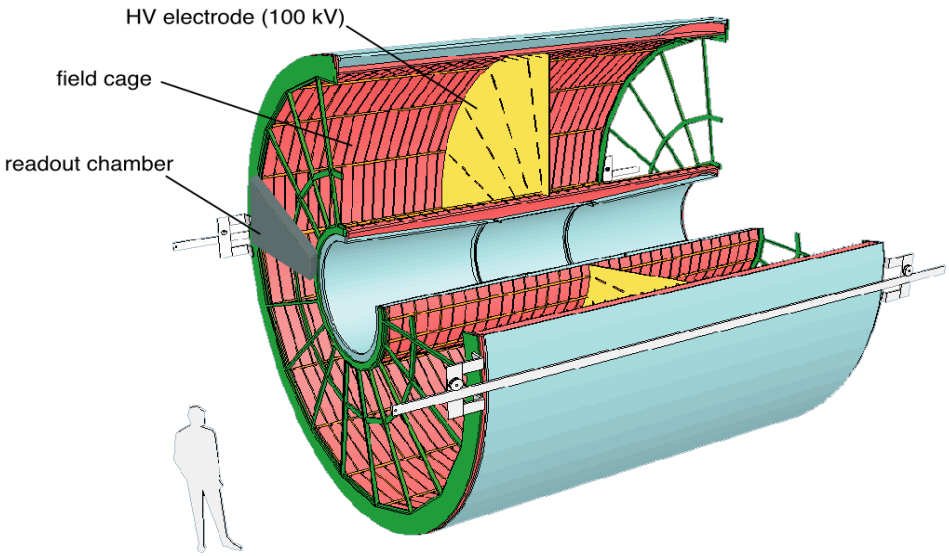


Figure 2.2: The ALICE TPC

| | |
|---|---|
| length | 5.5m |
| inner and outer radius | 0.80m - 2.5m |
| gas volume | 88m$^3$ |
| gas mixture | 90% Ne 10% $CO_2$ |
| central electrode voltage | 100 kV |
| field strength | (400V cm$^{-1}$) |
| drift velocity | 2.84 cm $\mu$s$^{-1}$ |
| Maximum drift time | 88$\mu$s |
| Number of detector pads | 557 568 |
| Sampling frequency | $5 - 10$ MHz |
| Maximum pad occupancy | 40% |

Table 2.1: List of the most important characteristics of the ALICE TPC [3]

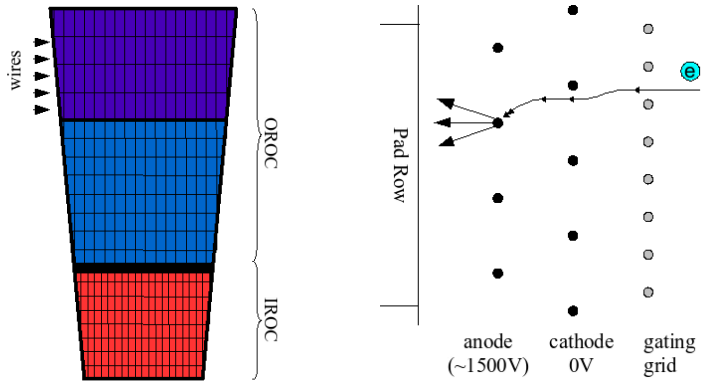


Figure 2.3: left : the 3 parts of a sector (IROC, OROCmedium, OROClong). There are in reality 4 times more pads, but the relative size in the different parts is correct. right : schematics of a wire chamber (here an OROC). The potential gradient between the cathode and the anode will accelerate the incoming electron and induce a localised ionization avalanche around the anode wire on collision with the gas. The gating wires have alternate potential when the gate is closed.

### 2.3.2 The Wire Chambers

The readout chambers used to detect the electrons are called MultiWire Proportional Chambers (MWPC). They amplify on the anode wire the incoming electrons in an ionization avalanche proportional to the number of electrons with a gain around 20 000. The avalanche will then be detected by an array of readout pads on the cathode. The chambers are divided in 18 sectors on each side of the TPC, and each sector is composed of two chambers (see Fig. 2.3) :

**The Inner ReadOut Chamber (IROC)** has 64 rows of $7.5 \times 4$ mm$^2$ pads.

**The Outer ReadOut Chamber (OROC)** has 64 rows of $10 \times 6$ mm$^2$ pads and 32 rows of $15 \times 6$ mm$^2$ pads.

The pads are smaller closer to the collision point to ensure a better resolution where the track density will be higher.

The MWPC consists of three wire grids with different potentials located above a readout plane with copper pads.

pad plane : 0 V

anode plane : $\sim$ 1500 / 1800 V (IROC / OROC)

cathode plane : 0 V

gating grid : $V_G = -100$ V (open gate) or alternate $100 \pm 80$ V every second wire (closed gate)

The large potential gradient close to the anode will accelerate the electrons coming from the drift volume. They will then hit with high energy some of the gas molecules and knock out more electrons to create an "avalanche" of ionization, freeing ions. The potential difference between the anode wire and the pad plane will drive the ions to the pads. The electrons will be picked up by the anode wire inducing a small signal on the pads while the ions will induce a larger signal as they move away from the anode. The induced signal is spread

over several pads. As the ions will move rather slowly, the charge deposit on the pads will have a long tail. The treatment of these effect will be discussed more precisely in section 2.3.3.

The gating grid is a device that will protect both the wire chamber and the drift volume by isolating them from each other when the detector is idle. In the *open* position, all the wires in the gating grid have the same potential, corresponding to the potential in the drift volume, and are then almost invisible to the electrons. In the *closed* position, the wires have alternate potential, creating a dipole field. This will prevent the electrons from the drift chamber to come to the amplification wires when there is no valid trigger, reducing the charge deposit on the anode wires. But more importantly, it also prevents the ions freed in the avalanche process from entering the drift volume and disturbing the electric field.

The switch from *closed* to *open* will produce a pulse in the pads (visible at the beginning of the raw data plots in chapter 3). Therefore, data in the first microseconds of the pad signal will not be used.

### 2.3.3 Pad Response

As mentioned before, the signal received at the pad level from a single electron will be distributed on several pads. The induced charge distribution, averaged over many avalanches, is called the "Pad Response Function" (PRF). The concept of PRF is generalised to the pad response in the general operating conditions of the detector, and will include diffusion and track parameters. It is an important parameter for the resolution of the TPC. Especially the two-tracks resolution since it is determined by the ability to separate overlapping clusters. The PRF is a systematic parameter strongly linked to the single coordinate resolution, but the resolution also includes statistical fluctuations. It is influenced by several effects (see [7]) :

**Pad Width** Theoretical studies (see [8]) showed that a pad width equal to twice the pad-anode distance gives a more or less gaussian PRF. In that case, the width of the gaussian is approximately half the width of the pad.

**Diffusion** The diffusion inside the drift volume will widen the cloud of electrons coming from an ionization point, and consequently widen the PRF. This augmentation will go with the square root of the drift length $l_D$.

**Track Angle** As a wire will collect the electrons coming from a segment of the track (as long as the distance $d$ between two wires), the PRF will depend on the length of the segment. This length is $d \tan \alpha$, where $\alpha$ is defined in figure 2.4. If we assume that the charge distribution is uniform along the track segment, the exact contribution will be exactly $\frac{L_{pad}^2}{12} \tan^2 \alpha$.

In the end, the PRF is a gaussian function with the following width :

$$\sigma_{PRF}^2(l_D, \alpha) = \sigma_{pad}^2 + \sigma_{diff}^2 + \sigma_\alpha^2 = \sigma_{pad}^2 + D_L^2 l_D + \frac{L_{pad}^2}{12} \tan \alpha^2 \qquad (2.1)$$

This formula will be important to evaluate the size of the clusters in the tracking algorithm (see 2.5.2), and the resolution of a cluster is roughly $\frac{\sigma_{PRF}^2}{\sqrt{N_e}}$ (where $N_e$

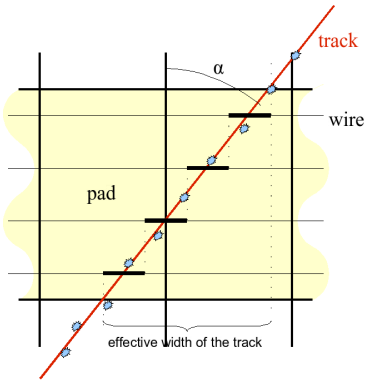


Figure 2.4: angular effect on the charge spread along the wires [7]

is the number of ionisation electrons.

The width of the time distribution is of course also influenced by the diffusion in the same way as the PRF. On the other hand, the shape of the signal in the time direction is dictated by the electronics.

## 2.4 Electronic Treatment of the Signal

The raw signal received by the pads is not usable directly. It must first be treated and digitalised by a chain of electronic processors.

### 2.4.1 PASA

As the signal is small (down to a few thousand electrons), it must first be amplified. This step, which includes some subtle treatment to correct base potential fluctuations, is performed by a PASA (**P**re**a**mplifier/**S**h**a**per). The amplification approximately turns a signal of 1000 electrons into one ADC channel, which corresponds to a gain of 12 mV/fC. The charge deposit on a pad has a specific time distribution with a long tail due to the slow drift of the ions. This signal is shaped by the PASA which turns the signal with ion tail into a higher and wider signal (cf figure 2.5) with a shaping time of about 200 ns.

### 2.4.2 ALTRO

The signal coming from the PASA still needs some corrections to be turned into usable data. The ALTRO chips (ALice Tpc ReadOut) perform a series of corrections to the digitised pulse.

**Digitisation** The ADC (Analog Digital Converter) transforms the analog signal from the PASA into a digitised signal with a sampling frequency of 5 or 10MHz.

**Baseline suppression 1** The baseline is uploaded and subtracted from the signal.

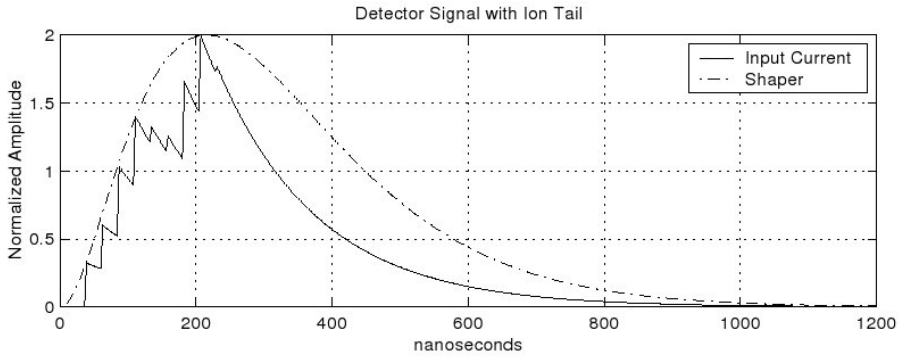


Figure 2.5: The ion tail component of each individual avalanche produces an integrated shape, then smoothed by the PASA [9]

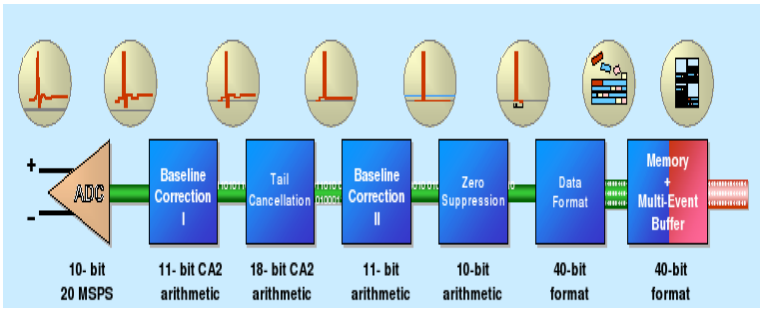


Figure 2.6: The chain of operations performed by the ALTRO chip

**tail cancellation** When the shape of the signal is known (uploaded in the chip), the tail can be extrapolated from the height. It can then be removed to more clearly separate the different contributions from close tracks.

**baseline suppression 2** The new baseline induced by the tail correction is suppressed.

**zero cancellation** The data with no signal (signal below threshold and far from a peak) is removed

For tuning purposes, some of these operations are not done on-line for the test. Therefore, the data extracted in this test experiment, that we will call "raw data", has offline (software) baseline correction and filtering, and contains all the time bins (no zero cancellation).

The complete readout chain is contained in the Front-End Cards (FEC). Each FEC contains 128 channels (i.e. pads). At most 32 FECs are controlled by a Readout Control Unit (RCU).

## 2.5 Data processing - Reconstruction

The raw data coming from the TPC is a digitised version of the charge as a function of time for each pad in the chambers. First, a clustering algorithm

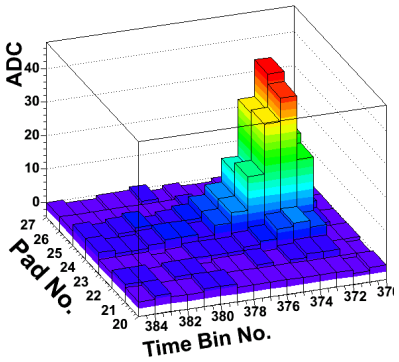


Figure 2.7: Raw data corresponding to a cluster. It is the time and pad charge distribution in a single row

transforms the raw data into small sets of cells (see fig. 2.7) called clusters corresponding to the original ionization events and to which are associated a certain number of characteristics. Then, a tracking algorithm is used to find the tracks.

### 2.5.1 Clusters

As seen in section 2.3.3, a single ionization event will leave a more or less gaussian charge pattern on several pads (usually 3 or 4). The signal on each of these pads is shaped by the PASA and digitalised by the ALTRO chip.

Figure 2.7 shows the form of the signal taken from the ALTRO for a few cells (time-pad bins). A cluster is clearly visible. A peak charge above a certain threshold (8 ADC) is required for each cluster. The cluster algorithm ([1] section 7.3.2) identifies this group of points and extracts the following values :

**Position** The radial position is defined as the number of the row where the cluster is (therefore it is discrete). The other two coordinates (Y and Z) are calculated as the centre of mass of the cluster, and are thus very precise numbers, even though the resolution is not that good.

**Position Spread** The widths of the clusters in Y and Z directions are given as the standard deviation (rms) in the cluster : $\sigma_Y$ and $\sigma_Z$

**Total Charge** This is the sum of the charges on all the pads in the cluster.

**Maximum Charge** This is the highest charge on a single cell.

The algorithm used for the test data limited the size of a cluster to $5 \times 5$ cells. For a 5 MHz sampling frequency, this represent a cluster size of $2(3) \times 2.5$ cm$^2$, which is large enough, but for the 10 MHz sampling frequency used in the test, it limits the time length of a cluster to less than 1.5 cm, which will frequently induce the loss of tail cells.

### 2.5.2 Tracking

Once we have reconstructed the original ionization points from the raw signal, we have to group the clusters into "tracks". This is an important and difficult step, due to the very high track density expected in ALICE. In the case of the cosmic test, the track density is for most events much lower than what is expected during the real experiment, but the tracks don't come from a single region, like in collision events.

The tracking algorithm starts by choosing a cluster from an outer row in the detectors (where the density is lower). From there, it looks for neighbouring clusters in the following row's plane. With these two points, one can extrapolate an angle, within which one should search for the next cluster. The determination of this angular range is dictated by the width of the first two clusters, and also by the theoretical error range (the pad response, see 2.3.3) of the next one, which will depend of the position and angle of the track.

Tracks respecting a certain number of criteria (for example, they must have more than a certain number of clusters) will be accepted. The coordinates will then be fitted with adapted functions (straight line in absence of magnetic field, circle arcs in its presence).

The tracking is the final step in data treatment before any physical interpretation, and its precision depends of the validity of the data and models for the clusters. It is therefore important to check this validity before the tracking process.

# Chapter 3

# Study of Irregularities in the Cluster Data

The approach used here in studying the data from the cosmic test was to focus on a few runs and study in detail the cluster data before the tracking.

Studying the data before the tracking allows to identify repetitive patterns from any systematic effect (e.g. noisy regions). These patterns might not be visible in clusters selected by the tracking algorithm, because of the low track density in the test. However, these effects will be more important in the high density environment of Pb+Pb collisions at LHC.

In that way, we can identify problems, understand them and correct or remove the data before performing the tracking.

## 3.1 Cosmic Test of the TPC

Before starting with the observations, I will describe the configuration used in the tests from which the data comes.

After the TPC had been assembled, a commission test program was run. The TPC was operated in a limited mode with only two sectors active at a time. Some tests used tracks obtained with the calibration laser which is part of the TPC. The others used cosmic rays : A set of scintillators was used to trigger on cosmic rays (see Figure 3.1). The different test runs activated different pairs of neighbour sectors, with different settings. In particular, the gain of the readout chambers was modified by changing the anode voltage.

The data studied here comes from some of the cosmic test runs. Each run lasted for a few hours during which a few thousands events (triggers) were recorded. I focus on four longer runs at the foreseen normal anode voltage of 1400V in the IROC and 1650V in the OROC.

## 3.2 Noise

Noise can appear in the dense front end electronics, coming either from the detector side or from the digital electronics. Noise at the input of the PASA (see section 2.4) could then be amplified and pollute the data. This would

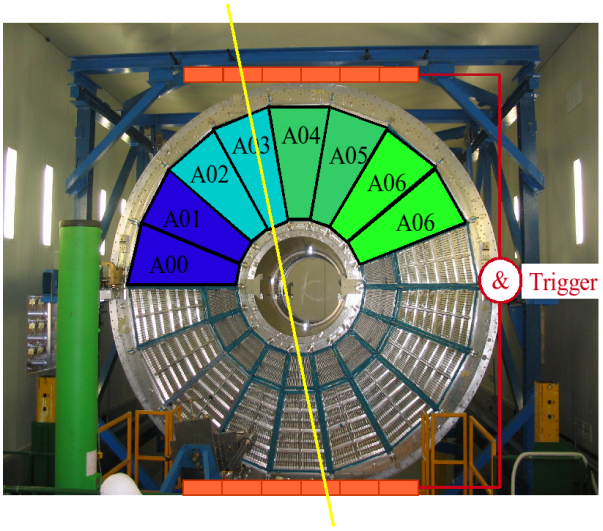


Figure 3.1: Setup for the cosmic ray test of the full TPC. Two sets of scintillators trigger on incoming rays. The sectors used for this study are highlighted.

result in baseline fluctuation that will, if high enough, pass through the zero suppression and modify or create clusters.

Noises with different origins, random or coherent, will be described here.

### 3.2.1 Edge Noise

Figure 3.2 (a) shows the clusters in a single event in one sector. The number of clusters (30 000 in a single event) is far too large (a track having at most 159 clusters). The distribution of the width in time of these clusters (fig. 3.2 (b)) shows that the noisy ones have a very small time spread, which is very improbable for real signal that is shaped by the PASA (see 2.4).

When we study the raw data (figure 3.3), we can see that it corresponds to a background noise on most of the edge pads. Looking more closely one sees that the baseline fluctuation is periodical with a high frequency (2.5 MHz = 4 time bins periodicity). The noise peaks are shorter than the PASA shaping time, which suggest that the source of the noise is followed by a signal of opposite polarity. The PASA output is therefore shorter than normal. This agrees with the small time spread of the noise clusters.

The structure of the noise (periodicity and phase) is exactly the same in all the chambers and in all events.

The observations of this noise led to a change in the grounding scheme for the OROC with less but thicker grounding cables. This new setting has been tested with pulser data and reduces the baseline fluctuations by a factor 2.

The data is written in the ALTRO 4 samples at a time. In a situation without zero suppression, this means that data is written simultaneously on all ALTRO with a frequency of $10/4 = 2.5$ MHz. This simultaneity should disappear when zero suppression is performed, and therefore data writing begins randomly. In any case, the setup of the electronics has been modified so that the ALTRO

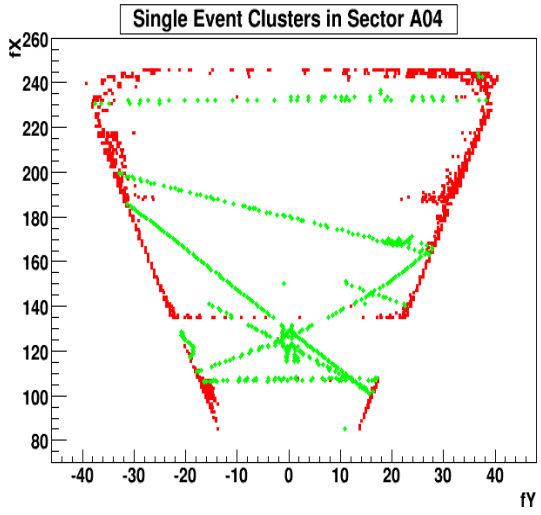


(a)

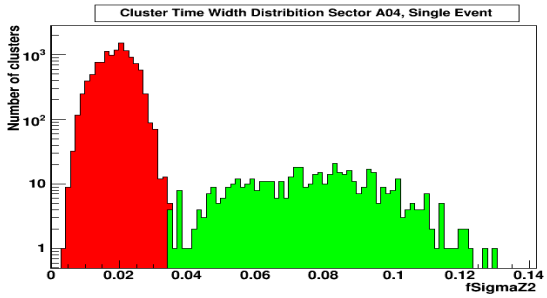


(b)

Figure 3.2: (a) Cluster distribution in a readout sector (IROC + OROC), for one event. (b) Time spread ($\sigma_Z^2$) of the clusters. The red clusters are high frequency noise, with $\sigma_Z^2 < 0.035$. Actual track clusters can be discriminated from the noise on the edges.

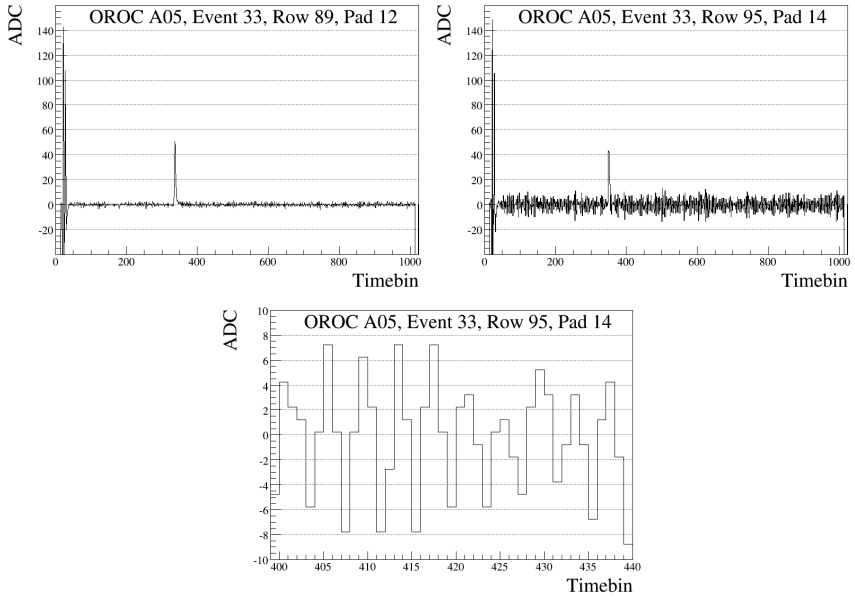


Figure 3.3: Signal on a detector pad, on the edge (upper right) and a little more to the centre (upper left). In both the track peak is visible. On the edge, the noise is periodical with high frequency At the beginning of the signal, the gate pulse (see section 2.3.2) is visible.

chips should not write on the same phase.

The combination of these two modifications significantly reduces the edge noise.

For the data available, most of the noise clusters can be cut by removing the clusters with small time spreads. This very efficient cut (as can be seen on figure 3.2, green points) allows to "clean up" the data, and make it "clean" for further studies. It gives a more efficient track finding and avoids the apparition of irrelevant noise tracks.

However, the data in the noisy region is modified by this noise, creating e.g. a bias in position. It is easy to imagine that clusters in the high frequency noise regions will more favourably be centred on a peak of the oscillations.
*All the cluster data used in the rest of this study is taken after making the cluster time width cut.*

### 3.2.2 High Density Regions

Once the edge noise has been removed, another problem can be seen. In the cosmic test runs, we expect a more or less uniform cluster distribution in the chamber. We thus look for unexpected behaviour, and then check whether it is systematic, and if we can find the reason for them.

On figure 3.4, we see small regions with a high cluster density (above 3 times the average). These anomalies can be localised to single pads. We must ignore these regions for further study of the test data, because, as they represent a

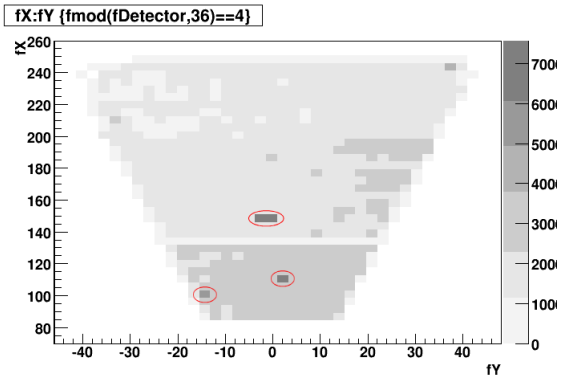


Figure 3.4: Cluster density in a readout sector : the small regions indicated by circles have a higher cluster density. We will call them "hot spots"

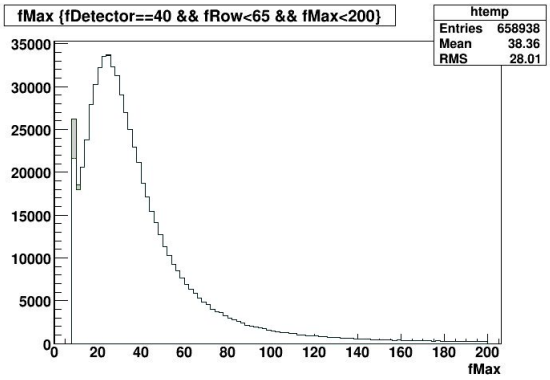


Figure 3.5: Maximum charge distribution in the OROC. In grey the contribution of the noisy region indicated in fig 3.4.

fair amount of the clusters, and have irrelevant characteristics, they can distort characteristics of the complete set, see Figure 3.5.

Figure 3.5 shows the contribution of the high density regions (which will also by referred to as "hot spots") to the charge distribution of the clusters. It is clear that these clusters, which don't follow the normal charge distribution, are noise. Three different kinds of hot spots are presented here.

### Low Frequency Noise

The first kind of noise is an unusually high random grounding noise on a single pad. It is difficult to know what the exact problem is. The signal is read out, but there is a large random background noise (see figure 3.6). There can probably be pads where there is only noise, and the signal is not read, but it is difficult to find events where one can be sure that there should be a signal on a very specific pad.

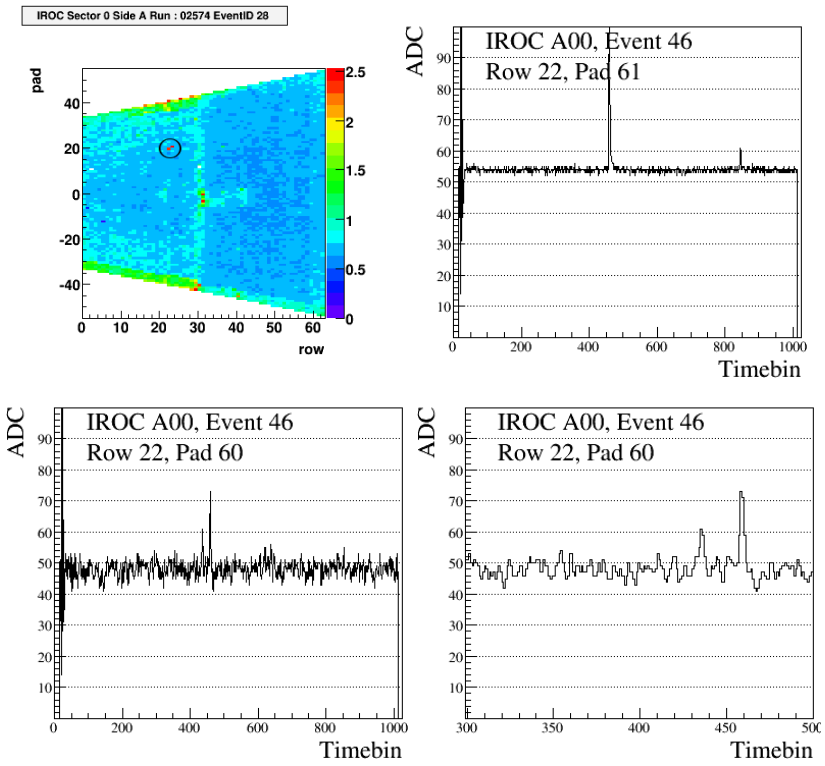


Figure 3.6: Up left : noise map (baseline rms) for IROC A00. The circle shows the region from where the other plots are taken. Up right : signal given by a normal pad with a track signal. Below : signal on a neighbouring noisy pad, same event, with the same track signal. A zoom on the noisy signal shows that it doesn't seem to have any regular pattern like in fig 3.3.

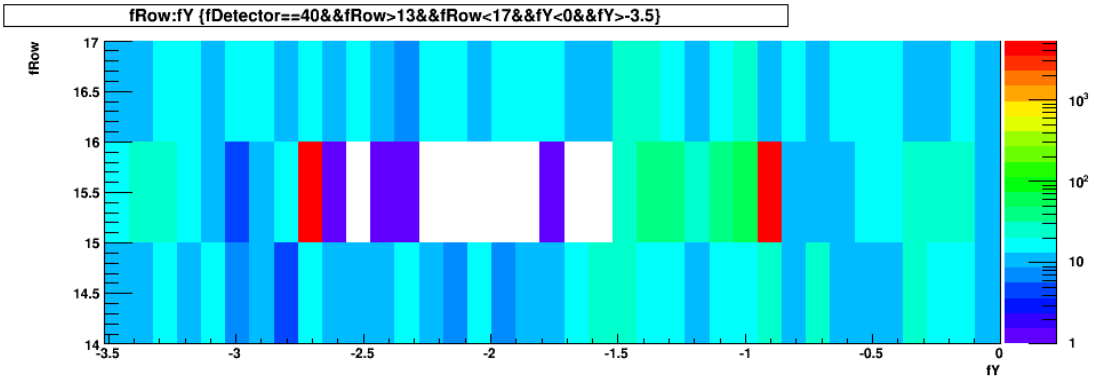


Figure 3.7: Cluster density around a floating pad (logarithmic scale)

### Floating Pad

For some particular high density region, when looking close enough, we actually see a low density region, enclosed between two high density regions (figure 3.7).

Figure 3.8 shows the corresponding raw data in an event where a track goes through this region. Four pads of a single row are responsible. The two middle pads don't show any signal of the track and have low baseline fluctuations. The two outer pads have higher noise (generating the noise clusters), and show a signal of the track exceptionally far from the track.

A lack of connection between the two middle pads and the electronics seems a probable explanation for this phenomenon. However the high gating pulse at the beginning of one of the silent pads signal is surprising in this hypothesis. A current leak between pads may also be considered, which would explain better the higher noise on the outer pads. This phenomenon is not yet fully understood.

### Ringing Noise

At the cluster level, the main particularity of these hot spots is that they are not only localised in space, but also in time. Looking at this noise more closely shows some sort of periodical "ringing".

Figure 3.9 shows that the noise in the considered region occurs only at the beginning of the event, so it seems that this noise is linked to the trigger that starts the data recording for one event and opens the gating grid.

In order to better understand the origin of this noise, we need to look at the raw data, i.e. the detector signal before clustering.

The raw data on Figure 3.10 shows that the baseline is not flat in the considered pads. This is probably due to saturation effects induced by the gate opening. The signal indeed comes in this region.

The ringing pattern with periodicity of 2.5 MHz can be the result of the small edge noise (section 3.2.1) on these pads. As all the time bins have approximately the same charge in this region, the small contribution of the 2.5 MHz edge noise will create a strong bias on the cluster position.

This noise should be removed by the on-line baseline correction in the ALTRO. Instead of subtracting a constant baseline, a more appropriate set of parameters will be used.

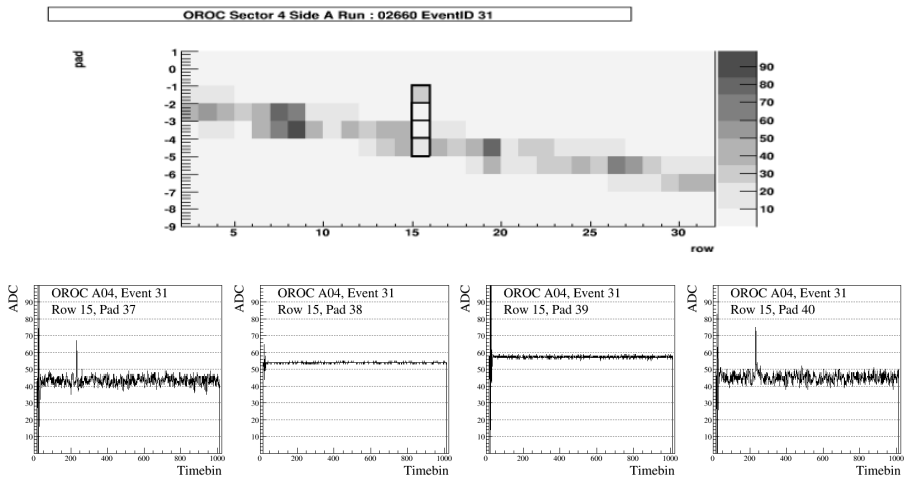


Figure 3.8: Above : trace of a track on the pads array as seen in raw data. Below : The signal read by the four highlighted pads. The two inner pads have low noise and no peak. The upper pad (right), though not very close to the track, has a surprisingly high peak. Both the "outer" pads have high noise.

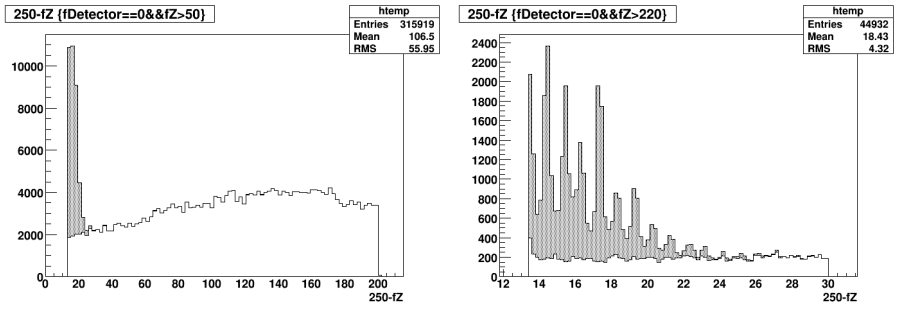


Figure 3.9: Cluster distribution in the z(=time) direction. In grey is the contribution of a very small region on the readout chamber. z is in cm.

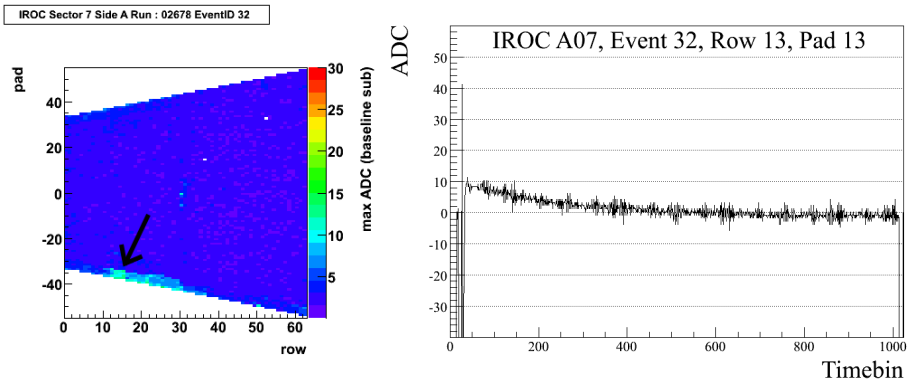


(a) (b)

Figure 3.10: (a) Signal received by the pads on the IROC for an event with no track (maximum signal after baseline subtraction). (b) Signal of the pad indicated by the arrow, after baseline subtraction, showing an exponential decay of the baseline

#### Other Hot Spots

At the centre of some IROCs, there are some hot spots. When we look at the raw data, it appears that there is a noisy region in the centre of every IROC.

The noisy region corresponds exactly to the border between asymmetric readout partitions. The difference of grounding and maybe also the clock shift between the RCUs for the two IROC partitions seem to induce a higher noise on the border pads.

### 3.2.3 Noisy Events

In order to have data as uniform as possible for further study, we also have to remove some unusual events, even if they are not noise. In a test run of several thousand of cosmic events some are extremely dense (up to a thousand times more clusters than usual).

Some are very high multiplicity cosmic ray showers. There are also corrupt events, which are results of firmware problems that are being fixed.

All the extremely high multiplicity events, corrupt or showers, should be studied separately, because they contain so many clusters that they bias the statistics. The shower events may perhaps be used for some specific studies, because they offer the possibility to understand the performance of the TPC in events which resemble Pb+Pb collisions at LHC.

### 3.2.4 Single Pad Clusters/Pad Response at the Cluster Level

When looking at the clusters distribution and properties at the pad scale, i.e. by using the position relative to the pad centres, one can observe some peculiar behaviours. The cluster distribution (see figure 3.13) shows a large amount of clusters right at the centre of the pads. This behaviour is clearly an artifact

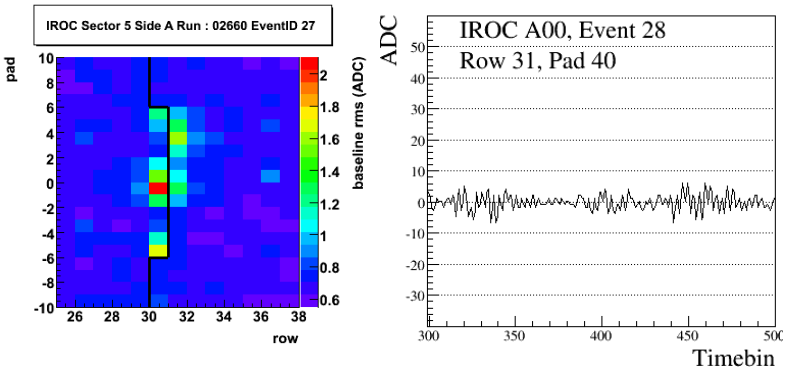


(a) (b)

Figure 3.11: (a) Noise map at the centre of an IROC : a set of noisy pads is visible where the border between the two read out partitions is asymmetric. (b) Signal from one of these pads : the baseline fluctuation seems periodical, with two periodicities : 3 time bins (3.3 MHz) and about 100 time bins (100 kHz)

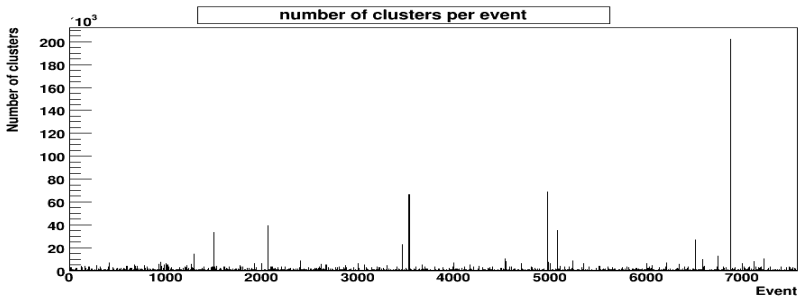


Figure 3.12: Cluster multiplicity as a function of event number. The spikes correspond to large cosmic ray showers.

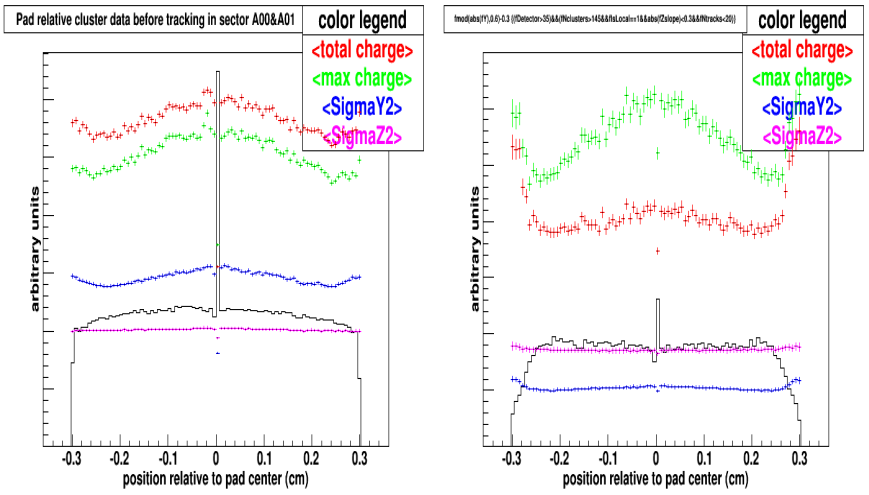


(a) (b)

Figure 3.13: Cluster distribution and properties with position relative to the pad centre (0 : centre of the pads, ±0.3 : edges). (a) from a horizontal sector (A00). (b) from a selection of perpendicular tracks in sector A04. The scales on both plots are the same. Single pad clusters (at the exact centre of the pad) are visible, though much reduced in the track data.

of the clustering, showing single pad clusters of which the position cannot be determined. They have very low charge and are assigned a width by the cluster algorithm. They also have a smaller width in the time direction, which also suggest noise origin. After track selection (see fig. 3.13 (b)), they are still present, but in smaller quantity.

They should probably be removed because the information they carry is not relevant.

Figure 3.13 also shows some non-uniform distribution of all the cluster characteristic except the time spread ($\sigma_Z^2$). This comes from complex statistical effects due to the small number of pads in a cluster.

For example, there are less clusters on the edges probably because it requires two pads with the same charge. This charge must be above the threshold of 8 ADC for the maximum charge in a cluster (see section 2.5.1). The edge cluster will thus be less common and with higher charge. Some effects are also suggested in the TPC Technical Design Report [1].

One can notice that in sector A00, where tracks have usually a small angle with respect to the wires, the distributions are more uniform. We have seen in section 2.3.3 that in this case, the clusters are bigger ($\sigma_Y^2$ large). They are consequently less affected by the statistical effects.

These effects should be studied in more detail than was possible in this short project.

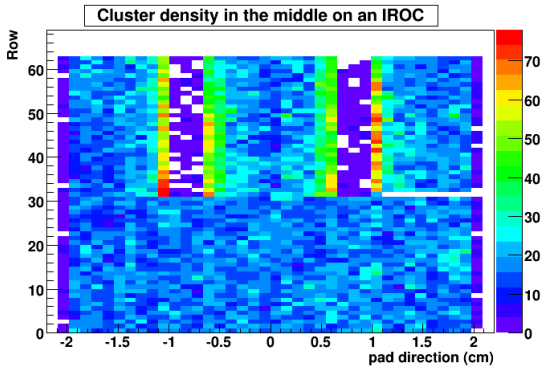


Figure 3.14: Cluster distribution in the central area of an IROC. A mapping problem introduced strange effect in the clustering

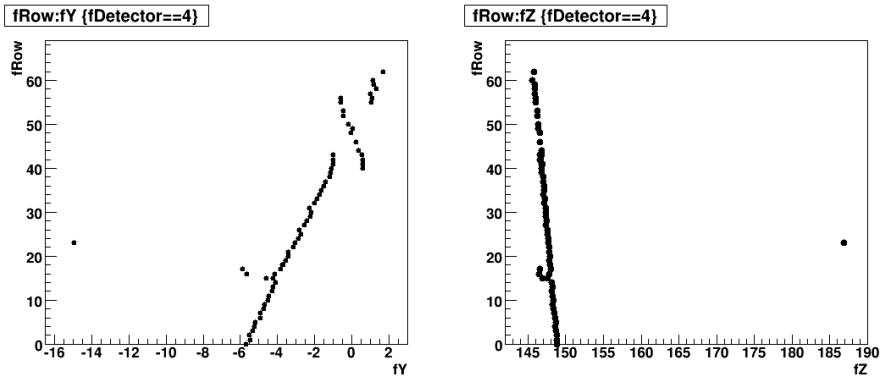


Figure 3.15: Display of an event in an IROC. There is clearly only one track on the (X,Z) projection (right) but there is reconstruction problem in the Y direction (left). One noise cluster can be seen. The small tail coming out of the track is probably a delta electron

## 3.3 Other Anomalies

Once we have cleaned the data, we can see finer anomalies.

### 3.3.1 Mapping problem in IROCs

On the cleaned data appears, on every sector at the same place, a non-uniform cluster distribution (figure 3.14).

The fact that this problem appeared on every sector suggest that it is an error in data processing rather than a material problem (The detectors having already been tested). By looking at a single event (and even a single track, figure 3.15) in the concerned region, one can see that there clearly is an error in the reconstruction of the clusters.

The pads in the central region have been given mirror coordinates in the pad mapping. Therefore, the clusters on the edges, being cut in half, are seen as two smaller clusters, explaining the “hot” lines in figure 3.14.

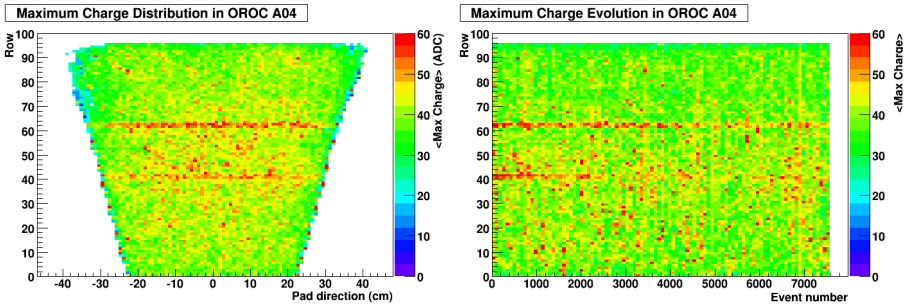


Figure 3.16: Mean maximum charge distribution on the (X,Y) plane (left) and the time (event scale for the whole run) evolution of its projection on the X axis. The two disconnected wires are visible as two high energy rows on the left plot. The effect fades with time, as seen on the right plot

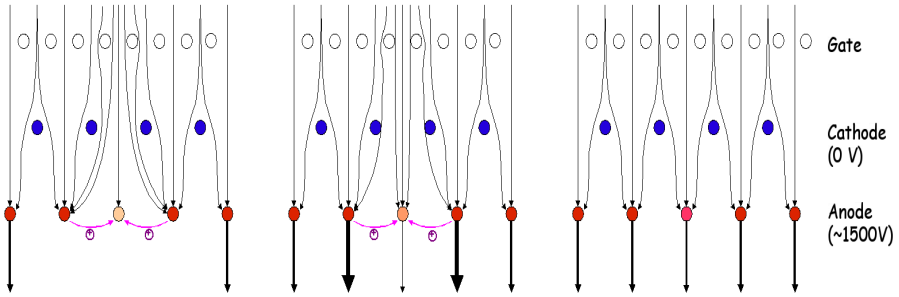


Figure 3.17: Possible explanation for the effect seen in the data in Figure 3.16. From left to right : charging up of a floating anode wire. Electrons trajectories are represented by the thin arrows, the thick arrows represent the strength of the amplification.

### 3.3.2 Floating wire on OROC4

The distribution of the mean total charge of each cluster on the surface of the OROC in sector A04 shows that two sets of neighbouring rows get a higher charge. When one studies the long term time evolution, it seems that this increased gain slowly disappears with time (see figure 3.16).

The increased gain can be explained by a disconnected anode wire. If an anode wire has a floating potential, it will create a greater potential gradient towards the two neighbour wires. This increased gradient will increase the gain around these wires, and consequently on the corresponding pad rows.

Now one can imagine that some ions will still drift around the wire and charge it up. The potential of the wire would then increase, reducing the effect. An illustration of this process is shown on figure 3.17. Other studies have shown that if the gating grid is opened randomly the higher gain remains. Incoming signal seems therefore needed for the effect to fade, which supports this hypothesis.

# Chapter 4

# Characteristics of Clusters in Tracks

In this chapter, some of the characteristics of clusters in tracks are measured and compared to theoretical expectation. For time reasons, I have restricted my study to the tracks in sector A04, where the trigger conditions are optimal (see figure 3.1).

To have no overlapping clusters, we only keep tracks from low multiplicity events (with less than 20 tracks).

When the dependence on track angle is not studied, in addition to this cut, the following cuts were applied :

- To reduce the angular effects in the cluster resolution (section 2.3.3) and the charge distribution, we can select tracks with low angle (radial tracks).
- To have more relevant track data, we keep only "long" tracks, with more than 145 clusters (out of the maximum 160 rows).

## 4.1 Evolution of the Cluster Width With Drift Length

As described in section 2.3.3, the size of the clusters is influenced by diffusion, so that $\sigma_Y^2$ and $\sigma_Z^2$ have a part proportional to the drift length $Z$.

$$\sigma_Y^2(l_D, \alpha) = \sigma_{pad}^2 + \sigma_{diff}^2 + \sigma_\alpha^2 = \sigma_{pad}^2 + D_L^2 l_D + \frac{L_{pad}^2}{12} \tan^2 \alpha \qquad (4.1)$$

$\sigma_{pad}$ depends only of the pad and wire geometry, and is 0.3 cm in OROCs and 0.2 cm in IROCs. The diffusion constant $D_L$ is quoted in [1] to be 220 $\mu$m cm$^{-1}$.

Figure 4.1 shows the cluster width dependence on drift length in time and pad directions.

The slope for $\sigma_Z^2$ is smaller than for $\sigma_Y^2$. This can be explained by the saturation of the cluster size in the time direction (see fig 4.2). Indeed, as seen in section 2.5.1, the size of the clusters is limited to $5 \times 5$ cells, which corresponds to 2 cm (3 cm) in pad direction in IROCs (OROCs) and only $\approx$1.3 cm in the time direction.

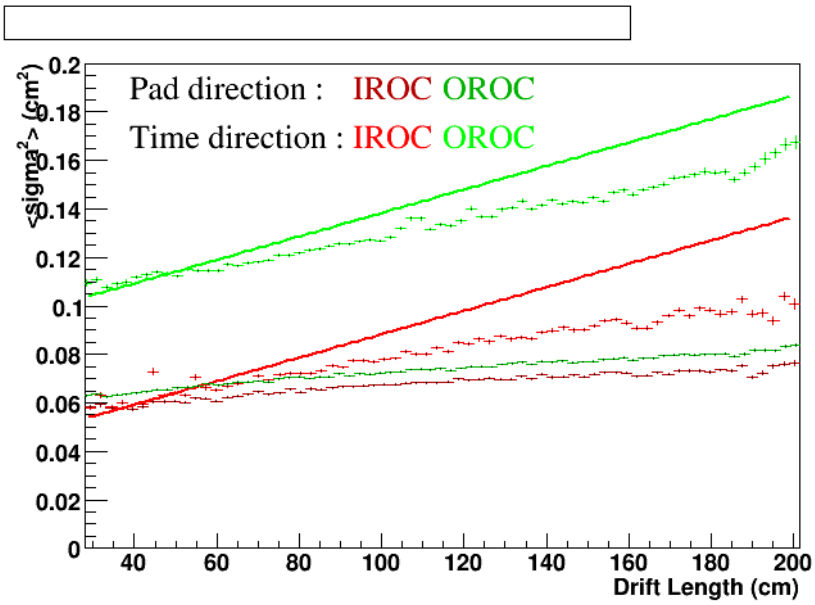


Figure 4.1: Evolution of the cluster width with drift length. The line is the expected evolution for $\sigma_Y^2$. $\sigma_Z^2$ should have the same slope, with the same origin in both IROC and OROC.

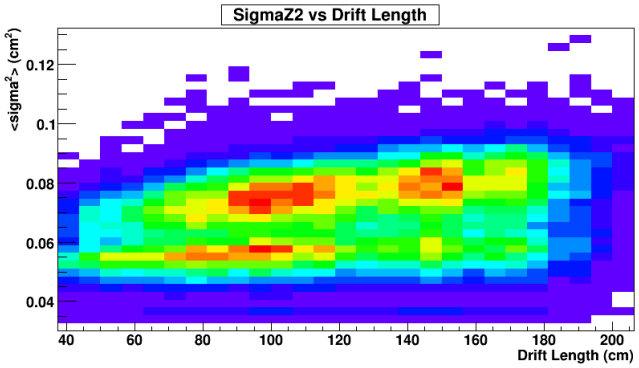


Figure 4.2: Distribution of the cluster time width and drift length. There is a saturation around 0.1 cm$^2$, which corresponds to a uniform distribution over the 5 time bins.

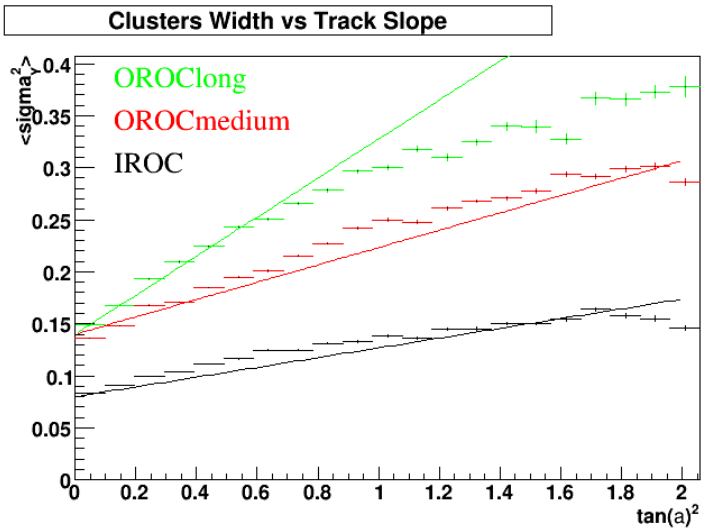


Figure 4.3: Evolution of $\sigma_Y^2$ with $\tan^2\alpha$ in the three parts of a sector (IROC, OROCmedium and OROClong). The solid lines represent the expected slopes (see eq. 4.1), with an offset adjusted to fit the data at low angle

However, the data from the IROC and OROC are consistent. The slopes are the same. The time spread is almost the same, as expected, with clusters a little bigger in the OROC, due to a larger track segment length corresponding to each cluster. $\sigma_Y^2$ is larger in the OROC where the pads are wider.

## 4.2 Evolution of the Cluster Width With Track Angle

Equation 4.1 shows that $\sigma_Y^2$ varies with $\tan^2\alpha$, whereas $\sigma_Z^2$ is not influenced by that angle. The angular dependence of $\sigma_Z^2$ doesn't seem relevant due to the strong saturation seen in section 4.1. Figure 4.3 shows the evolution of $\sigma_Y^2$ with $\tan^2\alpha$ in the three parts of a sector (IROC, OROCmedium and OROClong).

The theoretical lines on the figure include an ad hoc contribution of diffusion to fit the data at low angle. The data is in good agreement with the theory, for the small angles considered here. For an angle of 45°, i.e. $\tan^2\alpha = 1$, the track covers a number of pads $N_{pad} = \frac{L_{pad}}{l_{pad}}$. This makes 2.5 for the long pads, 1.67 for the medium and 1.75 for the short. The chances to reach the cluster saturation of 5 pads are therefore high for the long pads when $\tan^2\alpha > 1$.

## 4.3 Evolution of the Cluster Charge With Drift Length

Some of the ionisation electrons will be absorbed in the gas during the drift period of the electrons. According to [1] section 7.2.1.1, the losses of electrons in the drift volume is 1% per meter per ppm of $O_2$. We will thus expect an

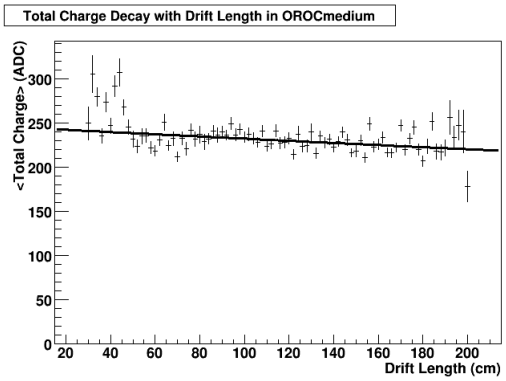


Figure 4.4: Decrease of the total charge of the clusters with drift length. The test data is fitted with an exponential.

exponential decrease of the total charge of the clusters with drift length. The cuts performed on the data (especially the angular cuts) insure a similar charge behaviour of all the clusters in one sector with the same pad length.

Figure 4.4 shows the evolution of the total charge of the clusters with drift length. The exponential fit give a loss of 5.3% $m^{-1}$, which would correspond to 5.3 ppm of $O_2$ in the gas. This is an upper value because as we have seen in section 4.1, some charge contributing cells are lost in the clustering algorithm. This value is in agreement with the expected 5 ppm [1], which shows that the field cage is tight and the gas system is efficient.

# Chapter 5

# Conclusion

By analysing the clusters from the first cosmic test data collected with the complete ALICE TPC, I have participated in identifying some irregularities. The edge noise has been reduced by a new grounding and electronic setup. The mapping problem in the IROCs has been fixed. The floating wires will need a further study to see if the gain modification can be corrected or if the rows must be ignored in the experiment. The isolated noisy pads will have to be removed or handled correctly by the tracking.

All these modifications and improvements is a step toward optimising the TPC and the reconstruction software for the challenges at LHC.

The short time scale of this project restricted the study to eight sectors, and a more complete and systematic study, with the help of the latest tools (monitors, reprocessed data, etc...), would be interesting for studying and understanding the TPC performance.

# Bibliography


[1] ALICE Collaboration. Time projection chamber technical design report. Technical report, CERN, 2000.

[2] ALICE Collaboration. Alice technical proposal. Technical report, CERN, 1995.

[3] ALICE Collaboration. Alice physics preformance report volume i. *Journal of Physics G*, 30(11), 11 2004.

[4] ALICE Collaboration. Alice physics preformance report volume ii. *Journal of Physics G*, 32(10), 10 2006.

[5] ALICE TPC Collaboration. Performance studies with an alice tpc prototype. *Nuclear Instruments and Methods in Physics Research*, 565:551–560, 2006.

[6] David d'Enterria. Quark gluon matter. *J. Phys. G: Nucl. Part. Phys*, 11 2006.

[7] Thomas Lohse and Werner Witzeling. The time projection chamber. Technical report, C.E.R.N, 1991.

[8] F. Sauli. The time projection chamber for heavy ion collisions: Trends and perspectives. *Z. Phys.*, C38:339, 1988.

[9] Bernardo Mota. *Time-Domain Signal Processing Algorithms and their Implementation in the ALTRO chip for the ALICE TPC.* PhD thesis, Ecole Polythechnique Fédérale de Lausanne, 5 2003.